IEEE Access
Multidisciplinary | Rapid Review | Open Access Journal

Date of publication xxxx 00, 0000, date of current version xxxx 00, 0000.

Digital Object Identifier 10.1109/ACCESS.2017.Doi Number

Investigation on Rotated Rectangular Slots to Improve the Circular Polarization in Cylindrical Dielectric Resonator Antenna

Reena Kumari[1], Ravi Kumar Gangwar[2], Senior Member IEEE and Raghvendra Kumar Chaudhary[3], Senior Member IEEE

Department of Electronics Engineering, Indian Institute of Technology (Indian School of Mines), Dhanbad 826004, INDIA

Corresponding author: Reena Kumari (e-mail: reena.31.dec@gmail.com).

"This research work is supported by science and Engineering Research Board (SERB), DST, India under project no. YSS/2014/000841".

ABSTRACT To achieve wideband circular polarization (CP) characteristics, a new structure with a single feeding technique has been proposed. In the proposed CP structure, to excite the cylindrical dielectric resonator (CDR) four asymmetrical rectangular slots are etched on the ground plane, each rectangular slot is rotated by an angle of ($\theta = 30^0$) with respect to its adjacent slots. The electric fields at each slot are separated by 30^0 in space with respect to its adjacent slot to create a 90^0 angular separations between the E-field components. Two orthogonal broadside modes ($HE_{11\delta}$) are excited inside the cylindrical dielectric resonator antenna (CDRA) independently to obtained CP characteristic. To compare the simulated outcomes with the experimental results, fabrication of the proposed antenna prototype has been done. The measured percentage of bandwidth achieved by the proposed radiator for $|S_{11}|$ and CP is 26.73% and 23.59%, respectively, and the whole usable axial ratio (AR) frequency bands overlap the impedance passband of the presented CP structure. The proposed radiator has achieved the maximum gain and radiation efficiency of 3.4 dB and 95% over the operating frequency range of the designed antenna, respectively. The proposed CP DRA has been configured for the WLAN band application.

INDEX TERMS Axial Ratio, Circular polarization, Dielectric resonator antenna, Wideband

I. INTRODUCTION

The inherent properties offered by dielectric resonator antenna (DRA) is found an appropriate selection for antenna designers due to its high radiation efficiency, small size, light weight, wideband, and easily excited with various feeding mechanisms [1, 2]. Circularly polarized (CP) DRAs overcome the limitations of linearly polarized (LP) DRAs due to their remarkable features such as the CP systems are insensitive to the problems of antenna misalignment and propagation effects, suppress multipath fading effect and better mobility in any weather condition [1-5]. Due to all these properties, CP DRAs are broadly applicable for satellite applications, mobile communications, navigation systems and radar [5, 6]. Several feeding mechanisms are presented in the literature for CP operation in DRAs they are single-fed [6], dual or multi-point fed [7 - 9] and sequential rotation feeding technique [10, 11]. The major difficulties found in designing the CP DRAs are maintaining the entire AR passband over the required impedance passband. Therefore, very few designs are available in the literature which has the axial ratio (AR) bandwidth completely covered by its impedance bandwidth. Some designs are reported in the literature such as cross-slot fed square DRA with an overlapping axial ratio bandwidth of 46.9% [12] and a square DRA excited by dual feeding configuration with an overlapping AR bandwidth of 43.5% [13] but due to dual feeding and large antenna dimensions, both structures become complex and bulky, respectively. A square DRA excited by a cross-slot was also stated with an overlapping AR bandwidth of 22.8% [14]. To generate CP wave by modifying the DR shape or geometry has also been carried out in the reported literature and they are a bow-tie shape DR [6] and cylindrical ring DRA [15]. Therefore, it is a very well-known fact that the ceramic material is very hard in nature due to that it is very difficult to modify its shapes or geometry. Another drawback, it costs more for any special DR geometry or shapes and not easily available in

This article has been accepted for publication in a future issue of this journal, but has not been fully edited. Content may change prior to final publication. Citation information: DOI 10.1109/ACCESS.2021.3093898, IEEE Access

the commercial market. All these modified shape structures [6, 15] are very complex as well as bulky.

In the present article, an innovative technique has been proposed for generating the CP wave by exciting the cylindrical DR with asymmetrical bow-tie shape slot along with off-centered microstrip feed without any modification in DR geometry or shape. These observations illustrate that the CP performance can be enhanced by single-point-fed regular-shaped DRAs by utilizing a proper feeding structure. In the proposed configuration, the total AR passband completely covered by its impedance passband with wideband CP performance. The complete AR frequency band is usable, which is another advantage. In TABLE-I performance comparison of the proposed antenna with some reported design has shown. So many wideband CP DRAs [12 - 15] are reported in the literature with complete overlapping between impedance and AR bandwidth but they are using complex DR geometry or shapes, multi-point feeding and large antenna dimensions due to that structures become very bulky and complex as compared to the proposed antenna.

TABLE I PERFORMANCE COMPARISON OF THE PROPOSED ANTENNA

Shape	f (GHz)	Dimension (mm)	Feeding	S_{11} (% & GHz)	AR (% & GHz)
Ring Cylindrical DRA [15]	26	13.2×13.2×1.524	Cross-slot substrate integrated	33.5 & (20.1-28.5)	26.3 & (20.3-26.45)
Square DRA [12]	2.3/3.4	76×76×19.8	Cross-slot	46.9 (2.19-3.53)	49.5 & (2.19-3.63)
Square DRA [13]	1.9/2.3/2.7	70×70×40	Dual Feeding	(1.7 - 3)	43.5 & (1.83 - 2.85)
Square DRA [14]	5/5.5	55×8.828	Cross-slot	25.4 & (4.8-6.2)	22.8 & (4.85-6.1)
Cylindrical DRA [Proposed]	5.5/6/6.5	46×46×10.1	Asymmetrical bow-tie shaped slot	26.73 & (5.25-6.87)	23.59 & (5.42-6.87)

II. ANTENNA GEOMETRY

A slot is etched in the ground plane and the complete slot is a combination of four asymmetrical rectangular-shaped slots. A rotation angle of ($\theta = 30^0$) is used to rotate each rectangular slot with respect to its contiguous slots. Since each slot has a 30^0 rotation with respect to its contiguous slots, therefore, a total angular separation of 90^0 is created by the four rotated rectangular slots. The geometrical form of the reported CP DRA is illustrated in Fig. 1. The presented design primarily comprises a cylindrical dielectric resonator (DR), a slot that is etched in the ground plane and a microstrip line. The relative permittivity of (ε_r = 9.8, tan δ = 0.002) is used as a cylindrical DR of radius 'R' and height 'H'. The FR4 epoxy of a dielectric constant (ε_{rs}= 4.4 & tan δ = 0.02) and dimension (L_s mm × W_s mm × t mm) is selected for the substrate. An off-centered 50 Ω microstrip line of length 'L' and width 'W' has been printed on the bottom layer of the substrate. The microstrip line is placed at a distance 'D' with respect to the center position of the substrate in the y-axis direction. With the help of the adhesive material, the cylindrical DR is positioned over the slot. The HFSS simulation software has been utilized to design and optimized the proposed CP radiator.

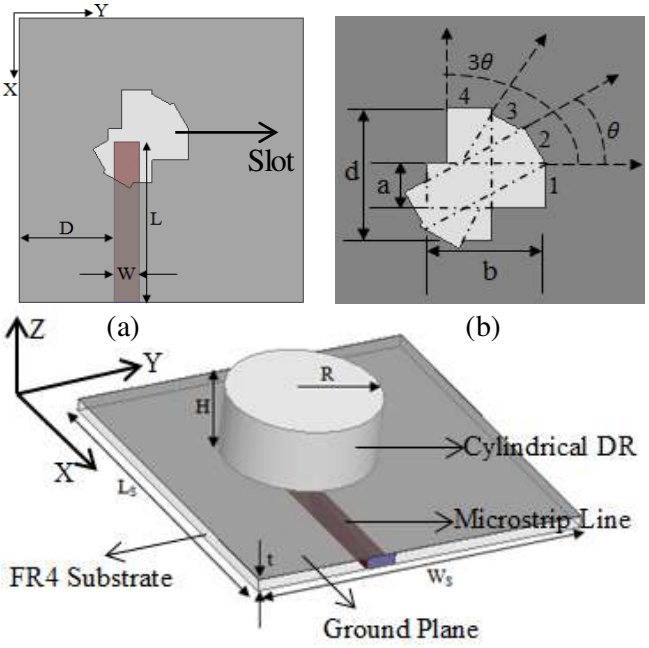

FIGURE 1. Geometrical representation of the designed antenna (a) Feeding Network (b) Slot Geometry (c) Side View. [L_S = 46 mm, W_S = 46 mm, t = 1.6 mm, R = 10 mm, H = 8.5 mm, L = 26 mm, W = 4 mm, D = 15.5 mm, a = 5mm, b = 13 mm, d = 15 mm]

III. ANTENNA ANALYSIS

A. EVOLUTION OF THE PROPOSED ANTENNA DESIGN

The present section deals with the evolution and theoretical background of the presented antenna design in two different approaches for CP generation, which are as follows.

Case I: (Horizontal slot to vertical slot): Fig. 2 describes the design procedure of the presented antenna in four different steps. Firstly, a cylindrical DR is fed by a horizontally placed rectangular *slot '1'* of dimension (*a* mm × *b* mm) referred to as Antenna 'W' shown in Fig. 2(a). On the next stage as shown in Fig. 2(b), along the azimuthal direction one another rectangular *slot '2'* of dimension (*a* mm × *d* mm) is introduced which is displaced by ($\boldsymbol{\theta} = 30^0$) in space with respect to the *slot '1'* in the counterclockwise direction named as Antenna 'X'. Due to that, ($\boldsymbol{\theta} = 30^0$) angular separation is formed between the excited electric fields at *slot '2'* and at *slot '1'* in space [16]. As shown in Fig. 2(c),

This article has been accepted for publication in a future issue of this journal, but has not been fully edited. Content may change prior to final publication. Citation information: DOI 10.1109/ACCESS.2021.3093898, IEEE Access

following the similar design process, by introducing rectangular *slot '3'* of the same dimension as *slot '2'* and it is separated by ($2\theta = 60^0$) rotation angle in space with respect to the *slot '1'*, Antenna 'Y' is formed. Due to that, again ($\theta = 30^0$) angular separation is formed between the excited electric fields at *slot '3'* and at *slot '2'* in space. In this way, through slot geometry modification, the direction of exciting electric fields have been decomposed inside the rotated slots [16]. Lastly, the proposed antenna 'Z' is designed by introducing rectangular *slot '4'* of similar dimension as *slot '2'* which is displaced by ($3\theta = 90^0$) with respect to *slot '1'* which is shown in Fig. 2(d). Therefore, electric field separation between *slot '4'* and *slot '3'* is 30^0 in space, between *slot '4'* and *slot '2'*, it is 60^0 in space and electric field at *slot '1'* is separated in space by 90^0 from electric fields at *slot '4'*. It has been observed that an angular separation of 90^0 has been created between the electric field components at *slot '1'* and *slot '4'* in space due to rotation of the different rectangular slots. In Fig. 3(a) and Fig. 3(b), four stages of different antenna configurations $|S_{11}|$ response and AR characteristics have shown respectively. It is important to note here that the non-orthogonal components of the electric field between contiguous slots such as *slot '1'* and *slot '2'*, or *slot '2'* and *slot '3'* and *slot '3'* and *slot '4'* also interfere with the far-field and thus worsens the CP bandwidth due to that in case of antenna structures (W, X and Y) no CP wave is excited which is shown in Fig. 3(b) [16]. For CP operation, the first requirement is to excite two linearly polarized orthogonal components of the electric field independently within the cylindrical DRA and the second condition is to create a 90^0 phase difference between these field components. So, the exciting electric fields have been disturbed by slot geometry modification along the counterclockwise direction and transformed into orthogonal field components (where, the angular separation between *slot '1'* and *slot '4'* is 90^0) in the final antenna stage [16]. Therefore, as the slot is moving from 0^0 to 90^0 in an anticlockwise direction, the minimum point of axial ratio in each antenna stage is also enhanced and reaches below the 3-dB point in the final presented antenna stage. In Fig. 4, E-fields are plotted at 5.84, 5.45, 5.6 and 5.4 GHz for antenna W, X, Y and Z, respectively, to check the decomposition with its top view of the rotating slots. The reported antenna is a hybrid DRA and the first resonant frequency is generated due to slot, justification of it has been discussed in a later section. In the hybrid DRA approach, the wideband features of the DRA are obtained by combining the frequency band of the two radiating elements of the antenna. Therefore, a wideband is generated due to the excitation of DR as well as radiation of the feeding network. So, the feed network has a major contribution to generating the wideband CP bandwidth; therefore, it excites the DR and also radiating its own in a predefined frequency range [5]. It has been observed that the $|S_{11}|$ bandwidth is increasing in every forward stage and the axial ratio minimum point is also enhanced from antenna 'W' to 'Z'. This is because with every forward stage, one rotated rectangular slot is embedded in the forward slot geometry due to that ground plane could be explored more modes that are suppressed by it. By introducing the more rotated slots, the hybrid structures excite the more number of resonance frequencies which are suppressed by the ground plane. On the final stage, a wide impedance and AR bandwidth of 27.01 % and 27.44 % are achieved by the proposed structure 'Z', respectively.

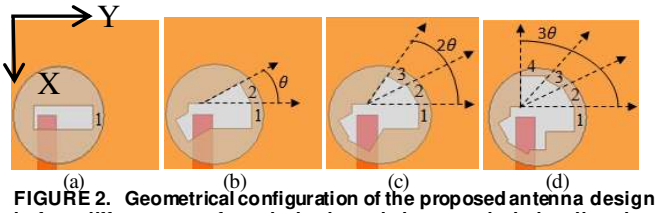

FIGURE 2. Geometrical configuration of the proposed antenna design in four different steps from the horizontal slot to vertical slot direction (a) Antenna 'W' (b) Antenna 'X' (c) Antenna 'Y' (c) Antenna 'Z' (Proposed design)

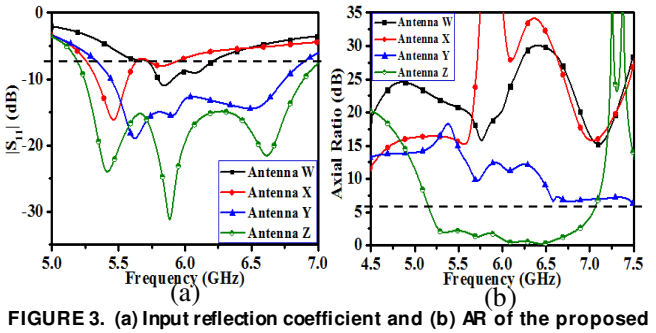

FIGURE 3. (a) Input reflection coefficient and (b) AR of the proposed antenna design in four different steps from the horizontal slot to vertical slot direction

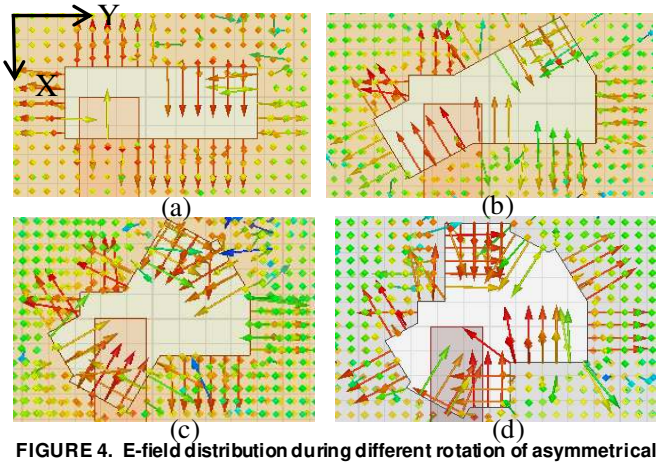

FIGURE 4. E-field distribution during different rotation of asymmetrical rectangular slots from the horizontal slot to vertical slot direction (a) Antenna 'W' at 5.84 GHz (b) Antenna 'X' at 5.45 GHz (c) Antenna 'Y' at 5.6 GHz (c) Antenna 'Z' at 5.4 GHz (Proposed design)

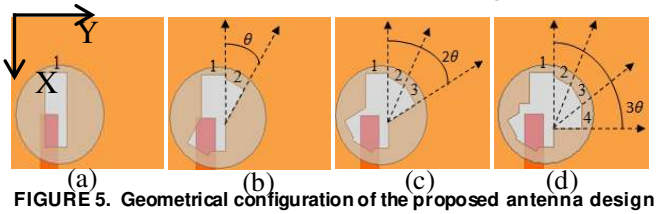

FIGURE 5. Geometrical configuration of the proposed antenna design in four different steps from the vertical slot to horizontal slot direction (a) Antenna 'P' (b) Antenna 'Q' (c) Antenna 'R' (c) Antenna 'S' (Proposed design)

This article has been accepted for publication in a future issue of this journal, but has not been fully edited. Content may change prior to final publication. Citation information: DOI 10.1109/ACCESS.2021.3093898, IEEE Access

Case II: (Vertical slot to horizontal slot): This approach is shown in Fig. 5 in four different steps and their respective $|S_{11}|$ and AR bandwidth curves are also shown in Fig. 6. In case II the concept of circular polarization mechanism is similar to the case I and it is already discussed in the previous section. Here, in this modification process, only the difference encountered is in every forward stage, the slot is displaced in space with respect to its adjacent slot in clockwise direction started from the vertically placed rectangular slot. When the different rectangular slots are rotated differently along the azimuthal direction like a spiral pattern, the different components of electric fields such as Eslot-1, Eslot-2, Eslot-3 and Eslot-4 are existing within the rotated slots due to the decomposition of the primary E-field. Therefore, different E-field components are separated with different angles in space due to the modification of slot geometry. This analysis is shown in Fig. 7 and Fig. 8, by plotting the E-field inside the rotated slots where each electric field component covers the different path lengths within the rotating slots. This introduces the required phase difference due to the different amounts of distance created between the orthogonal E-field components. A comparison table between case-1 and case-2 has shown in TABLE-II

TABLE-II Comparison table for case-1 and case-2

Case-1 Antenna	$\|S_{11}\|$ %	AR %	Case-2 Antenna	$\|S_{11}\|$ %	AR %
W	1.7	0	P	0	3.59, 2.15
X	4.03	0	Q	6.5, 2.86	0
Y	21.31	0	R	30.63	13.91
Z (Proposed)	27.01	27.44	S (Proposed)	27.01	27.44

In this perspective, various structures (Antenna A, B and C) based on different rotation angles 'θ' of the rectangular slots have shown in Table-III and their respective E-field distributions have also shown in Table-III. In Fig. 9(a) and Fig. 9(b), the reflection coefficient and AR variation for different antenna structures (A, B and C) have shown, respectively. From Fig. 9(a), it is noticed that if the rotation angle is increased first resonant frequency of the input reflection coefficient shifted in the lower frequency side. Therefore, the rotation angle directly affects the first resonant frequency because the presented antenna is a hybrid DRA and the first resonant frequency is generated due to the slot. From Fig. 9(b), it has been noticed that the AR bandwidth is not similar to all structures shown in Table-III, even the fields have been decomposed. Due to different angular separation between the adjacent slots, the axial ratio bandwidth of all three cases is also not similar. The electric field components inside the rotated slots cover the different path lengths. This also confirms the angular separation between the orthogonal components of the E-field inside the rotated slots entirely depends on angular separation 'θ'. In Table IV $|S_{11}|$ and AR results for different antenna design (A, B & C) with respect to different step angles 'θ' has shown.

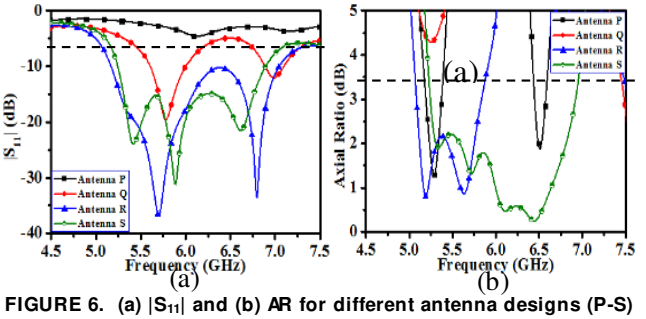

FIGURE 6. (a) $|S_{11}|$ and (b) AR for different antenna designs (P-S)

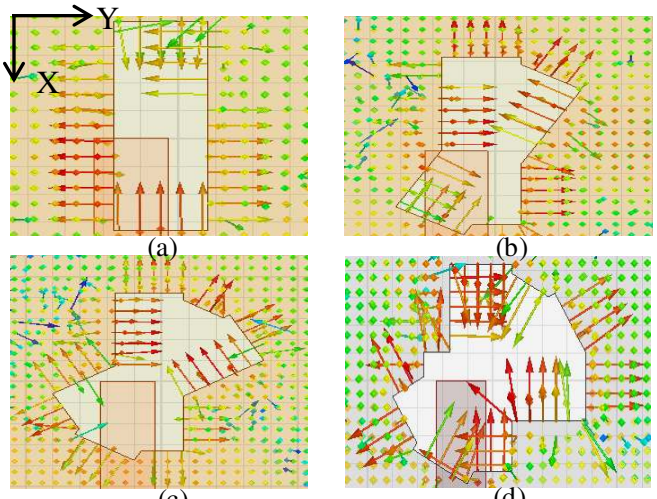

FIGURE 7. E-field distribution during different rotation of asymmetrical rectangular slots from the vertical slot to horizontal slot direction (a) Antenna 'P' at 5.28 GHz (b) Antenna 'Q' at 5.8 GHz (c) Antenna 'R' at 5.7 GHz (c) Antenna 'S' at 5.4 GHz (Proposed design)

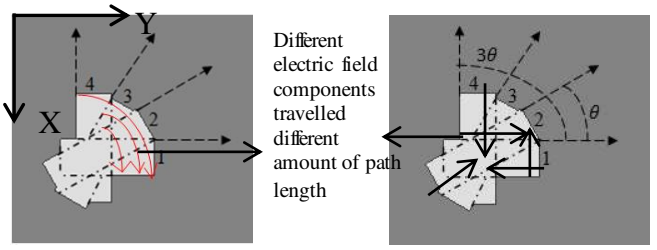

FIGURE 8. Different electric field components travelled different amount of path

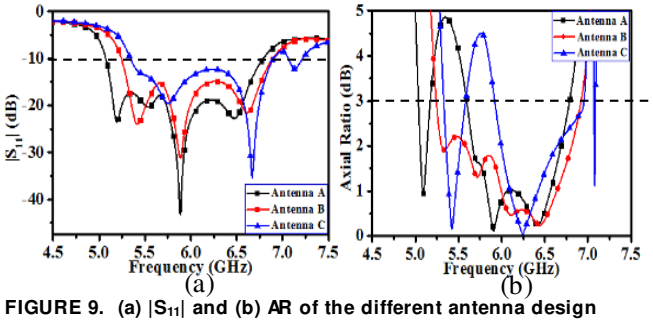

FIGURE 9. (a) $|S_{11}|$ and (b) AR of the different antenna design

This article has been accepted for publication in a future issue of this journal, but has not been fully edited. Content may change prior to final publication. Citation information: DOI 10.1109/ACCESS.2021.3093898, IEEE Access

TABLE III GEOMETRICAL CONFIGURATION OF THE DIFFERENT ANTENNA DESIGN WITH RESPECT TO STEP ANGLE '**θ**' AND E-FIELD DISTRIBUTION (a) Antenna 'A' at 5.75 GHz (b) Antenna 'B' at 5.4 GHz (Proposed design) (c) Antenna 'C' at 5.2 GHz

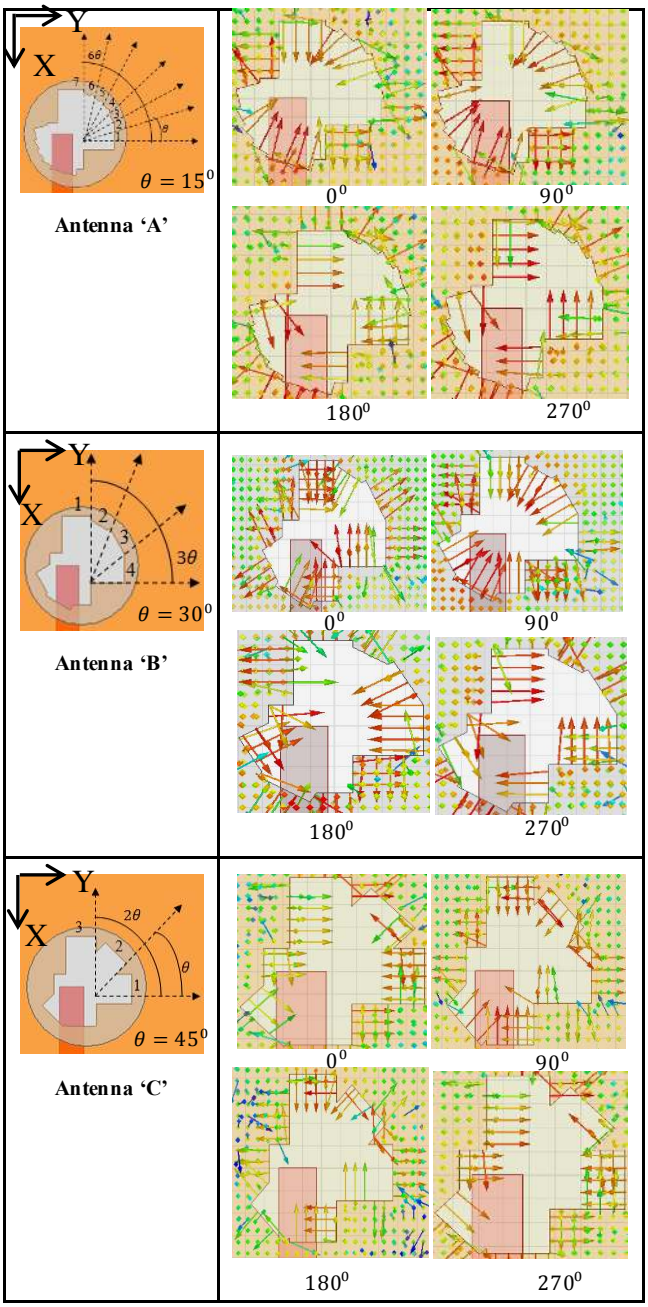

TABLE IV $|S_{11}|$ AND AR BANDWIDTH FOR DIFFERENT ANTENNA DESIGN (A, B & C) (SHOWN IN TABLE I) WITH RESPECT TO DIFFERENT STEP ANGLES 'θ'

Antenna	Impedance Bandwidth %	Axial Ratio Bandwidth %
A	28.66	(2.54 & 19.06)
B	27.01	27.44
C	(25.30 & 1.96)	(4.58 & 16)

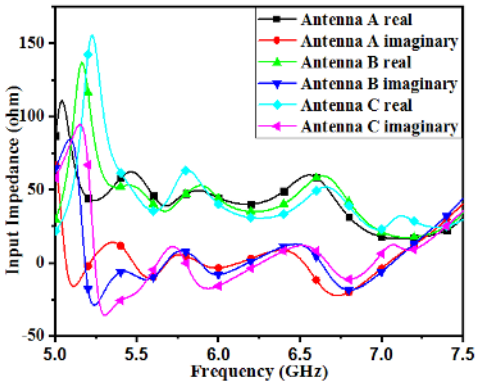

FIGURE 10. Input impedance versus frequency curve of the different antenna design

However, the resonant frequencies and the matching frequency ranges changed with different rotation angles between the consecutive slots. In this perspective, input impedance versus frequency curves of the different antenna designs (A, B and C) has shown in Fig. 10. Antenna-A (with 15^0 rotation angle), the matching frequency ranges are (5.08 - 6.78) GHz with resonant frequency at 5.19 GHz, 5.54 GHz, 5.89 GHz and 6.47 GHz. Antenna-B, (with 30^0 rotation angles), the matching frequency ranges are (5.25 - 6.89) GHz with the resonant frequency at 5.42 GHz, 5.89 GHz and 6.62 GHz. Antenna-C, the matching frequency ranges are from (5.35 - 6.9) GHz and (7.07 - 7.21) GHz with resonant frequency 5.75 GHz, 6.67 GHz and 7.13 GHz, respectively. This indicates that the resonant frequency is very sensitive to the rotation angle of the slot. So, it is observed that in each case the real and imaginary parts are near about 50 ohms and 0 ohm, respectively. In the case of Antenna-C, the resonant frequency is shifted more as compared to (Antenna-A and Antenna-B) and wider axial ratio bandwidth is achieved in the case of Antenna-B as compared to Antenna A and C.

B. GENERATION OF CIRCULAR POLARIZATION

In the proposed structure, two orthogonal modes of CDRA similar to $\mathbf{HE_{11\delta}}$ mode at 5.9 GHz and 6.6 GHz, respectively, are excited to achieve the wideband CP bandwidth. For introducing a 90^0 angular separation between the two linearly polarized E-field components, four rotated asymmetrical rectangular slots like asymmetrical bow-tie shaped are introduced. Therefore, rotated slots are introducing gradual orthogonality between the field components. The effect of DRA on input reflection coefficient and axial ratio response with respect to frequency has shown in Fig. 11. From Fig. 11(a) it is concluded that without DRA except the first resonant peak (5.4 GHz), the remaining two resonant peaks (at 5.9 GHz and 6.6 GHz) have vanished. Therefore, the first resonant peak is excited due to the slot and the remaining two resonant peak is coming due to CDRA.

This article has been accepted for publication in a future issue of this journal, but has not been fully edited. Content may change prior to final publication. Citation information: DOI 10.1109/ACCESS.2021.3093898, IEEE Access

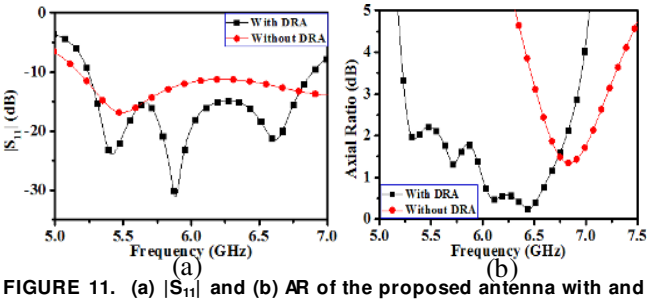

FIGURE 11. (a) $|S_{11}|$ and (b) AR of the proposed antenna with and without DRA

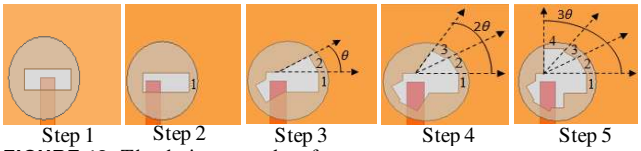

FIGURE 12. The design procedure for antenna prototypes

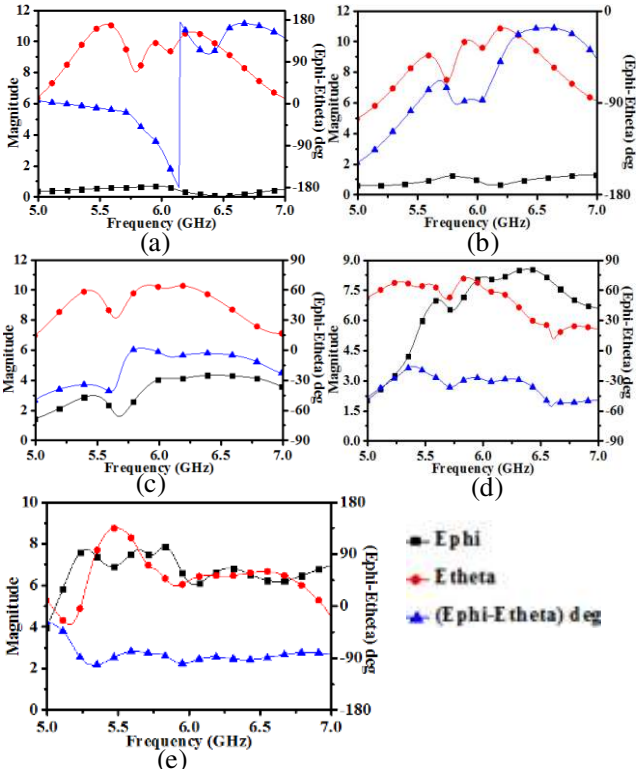

FIGURE 13. Simulated magnitude of the E-field components and angle between the E-field components in degree of all five stages of the proposed antenna configuration

The five design stages of the reported CP antenna have been shown in Fig. 12, to demonstrate the operating principle of the presented CP DRA. In Fig. 12, all the design parameters of the antenna structure were kept constant and on the ground plane rectangular slots are introduced step by step. The simulated graph of the magnitude of the E-field components (i.e. Ephi/Etheta) and angle between the Ephi and Etheta (in degree) with respect to frequency of all five stages of the proposed antenna configuration has shown in Fig. 13. To generate CP fields, these conditions must be fulfilled the two orthogonal linear components of the field must be presented with the same magnitude and must have a phase difference of odd multiples of 90^0. In stage 1, a cylindrical dielectric resonator (CDR) is excited by symmetric aperture feed i.e. the microstrip line is placed centrally with respect to the rectangular slot. But in this case, only one field component is excited, i.e. Ephi and Etheta~0 tend to zero magnitude. Therefore, it does not fulfill the CP condition. In step 2, to introduced the Etheta component, asymmetrical feed is used to excite the CDR which is shown in Fig. 12 and Fig. 13, respectively. In the third stage, i.e. step 3, rectangular slot '2' is introduced it will increase the magnitude of the Etheta component, but its magnitude is not equal to the Ephi component. Due to that slot '3' is introduced, it will again increase the magnitude of the Etheta component which approaches the magnitude of the Ephi component, but its magnitude is not equal to the Ephi component over the complete AR frequency range. In step 5, rectangular slot '4' is introduced, resulting magnitude of Ephi and Etheta is almost equal over the AR frequency range and 90^0 phase difference between the E-field components are also achieved.

C. PARAMETRIC ANALYSIS OF THE PROPOSED ANTENNA DESIGN

The $|S_{11}|$ and AR variation for different slot length 'd' has shown in Fig. 14(a) and 14(b). With an increase in slot length 'd', the first resonant frequency goes down in the lower frequency region as compared to the second and third resonant frequencies. The presented antenna is a hybrid DRA and the first resonant frequency is generated due to the slot. Therefore, any changes in slot dimension directly affect the first resonant frequency of the reflection coefficient response. Similarly, from Fig. 14(b), the AR bandwidth also minimizes if slot length varies from 14 mm to 17 mm and it becomes lower for d=17 mm. Therefore, to achieve maximum AR bandwidth, the slot length of d=15 mm is fixed for the final optimized design. Table V illustrates the $|S_{11}|$ and CP bandwidth for different lengths of the slot (d).

In Fig. 15(a) and Fig. 15(b), the effect of different slot width 'b' on $|S_{11}|$ and CP bandwidth is similar to slot length 'd' has shown. It is found that the greater CP bandwidth is produced for the case b=13 mm.

Fig. 16 explains the effect of the displacement (D) of the microstrip line along the y-axis direction. As 'D' increases from 14.5 mm to 17.5 mm, it affects the impedance matching of the reflection coefficient and also reduces the impedance bandwidth. In the case of AR, if 'D' increases or decreases, it is reduced to a lower value for both conditions. The maximum impedance and CP bandwidth have been produced for the case D=15.5 mm.

IV. EXPERIMENTAL RESULTS

On the basis of optimized parameters proposed in Fig. 1, a prototype of the presented CP design has been fabricated to verify the HFSS results. In Fig. 17, a clear picture of the fabricated DRA has been displayed. The measurement of the input reflection coefficient of the fabricated DRA has

This article has been accepted for publication in a future issue of this journal, but has not been fully edited. Content may change prior to final publication. Citation information: DOI 10.1109/ACCESS.2021.3093898, IEEE Access

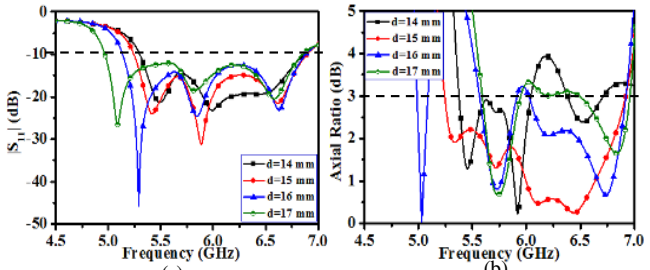

FIGURE 14. The effect of slot length 'd' variation on (a) $|S_{11}|$ (b) AR

TABLE V IMPEDANCE AND AXIAL RATIO BANDWIDTH FOR DIFFERENT SLOT LENGTH

Slot length (d) in mm	IM BW (GHz & %)	AR BW (GHz & %)
14	(5.3 – 6.87), 25.8	(5.38 – 6.04), 11.55 (6.38 – 6.71), 5.04
15	(5.25 – 6.89), 27.01	(5.25 – 6.92), 27.44
16	(5.14 – 6.88), 28.95	(4.99 – 5.08), 1.78 (5.57 – 5.91), 5.92 (6.03 – 6.92), 13.74
17	(4.97 – 6.85), 31.81	(5.6 – 5.94), 5.89 (6.5 – 6.96), 6.83

Where, IM BW=Impedance bandwidth, AR BW=Axial ratio bandwidth

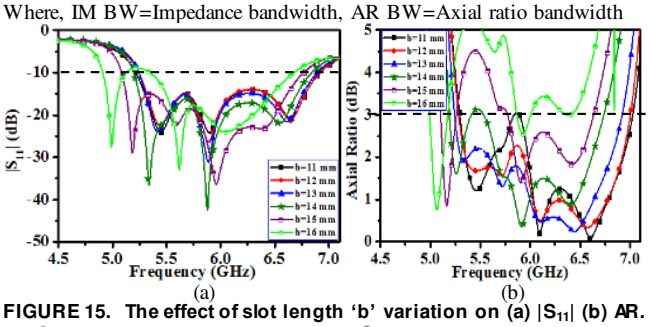

FIGURE 15. The effect of slot length 'b' variation on (a) $|S_{11}|$ (b) AR.

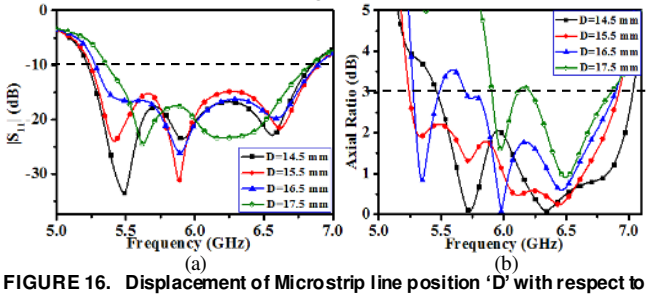

FIGURE 16. Displacement of Microstrip line position 'D' with respect to the center of the substrate in the y-direction (a) $|S_{11}|$ (b) AR.

been displayed. The measurement of the input reflection coefficient of the fabricated DRA has been done through the Keysight Performance Network Analyzer (PNA) N5221A (10 MHz - 13.5 GHz). Fig. 18(a) illustrates that the input reflection coefficient ($|S_{11}| < -10$ dB) response as a function of frequency. From Fig. 18(a) the simulated and experimental impedance bandwidth of 27.01% and 26.73% has been delivered by the presented structure, respectively. The reflection coefficient response shows that the novel agreement between the experimental and simulated curve. Some minor discrepancies occurred between the experimental and simulated outcomes which may be generated due to fabrication errors.

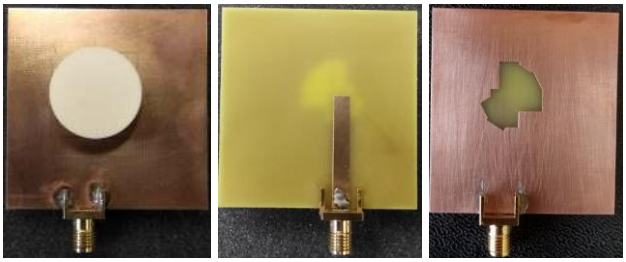

FIGURE 17. Fabricated antenna photographs (a) Top view (b) Microstrip feeding (c) Slot geometry

A. AXIAL RATIO

The far-field parameters have been measured along the boresight direction, i.e. (θ=0 and ϕ=0). Fig. 18(b) illustrates the simulated and experimental CP bandwidth of 27.44% and 23.59%, respectively. A slight difference is observed between the measured and simulated AR result which may be also created due to fabrication tolerances such as the use of adhesive material for placing the DR onto the slot which is not considered at the time of simulation and a slight displacement of DR from its exact position. Table VI illustrates the AR performance of the presented CP antenna according to the operating frequency ranges and % bandwidth.

B. RADIATION PATTERNS

For two planes, i.e. ($\phi=0^0$ and $\phi=90^0$), the proposed structure radiation pattern has been experimentally tested. Fig. 19 and Fig. 20 explain the simulated and experimental radiation pattern at 5.7 GHz and 6.4 GHz respectively, for two principle planes, i.e. (*xz* and *yz*) of the proposed antenna. From Fig. 19, at 5.7 GHz, the component of right-hand CP (RHCP) field is greater than the left hand CP (LHCP) field by 30 dB and 20 dB along the broadside direction in two principles (*xz*- and *yz*-) planes, respectively. Fig. 20 also illustrates that the proposed antenna radiation pattern at 6.4 GHz and the observation shows that the RHCP field is also greater than the LHCP field by 20 dB and 30 dB for both planes such as (*xz* and *yz*), respectively. Fig. 19(a) and 19(b) the beamwidth at 5.7 GHz is (82^0) and (60^0), respectively. Fig. 20(a) and 20(b), the 3-dB beamwidth at 6.4 GHz is (128^0) and (78^0), respectively.

C. SENSE OF POLARIZATION

The direction of rotation of the rectangular slot decides the sense of antenna polarization. Circular polarization can be generated by properly selecting the rotation angle of the

This article has been accepted for publication in a future issue of this journal, but has not been fully edited. Content may change prior to final publication. Citation information: DOI 10.1109/ACCESS.2021.3093898, IEEE Access

rectangular slot. Here, each slot is rotated by 30^0 with respect to its contiguous slots, therefore the total angular separation of 90^0 is created by the four rotated rectangular slots. The RHCP and LHCP conversion mechanism is shown in Fig. 21. According to Fig. 21(a) slot position, the RHCP field will be generated and by taking a mirror image of Fig. 21(a), the RHCP field is converted into the LHCP field which has shown in Fig. 21(b).

D. GAIN AND RADIATION EFFICIENCY

The experimental and simulated gain curve variation with respect to frequency has explained in Fig. 22 and the maximum measured gain of 3.4 dB is delivered by the presented CP antenna. Hybrid DRA is the combining effect of the dielectric resonator and some other radiating element in the antenna structure [18, 19]. This method provides the advantage of compactness along with independent control over the different frequency bands. But, it suffers from high fluctuation in gain value over the operating frequency bands [20]. Fig. 22 also discussed the radiation efficiency of the presented CP DRA with respect to frequency and the radiation efficiency of 95% has also obtained over the frequency range 5 to 7 GHz. A comparison table of the proposed antenna with other slot-fed DRAs has shown in TABLE VII and the proposed CP DRA shows better CP performance as compare to the listed CP DRAs in the below table.

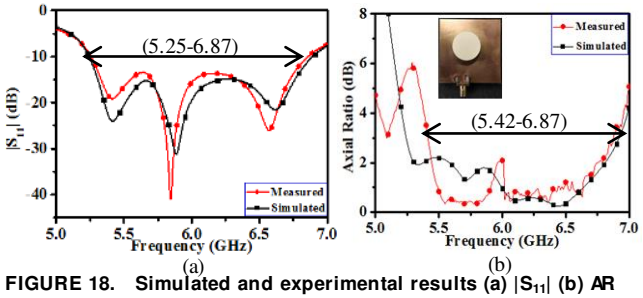

FIGURE 18. Simulated and experimental results (a) $|S_{11}|$ (b) AR

TABLE VI PERFORMANCE OF THE PROPOSED ANTENNA

Parameters	-10-dB Impedance Bandwidth		3-dB Axial Ratio Bandwidth	
	Simulated	Measured	Simulated	Measured
Operating Frequency Range in GHz	(5.25-6.89)	(5.25–6.87)	(5.25-6.92)	(5.42–6.87)
% Bandwidth	27.01 %	26.73 %	27.44 %	23.59 %

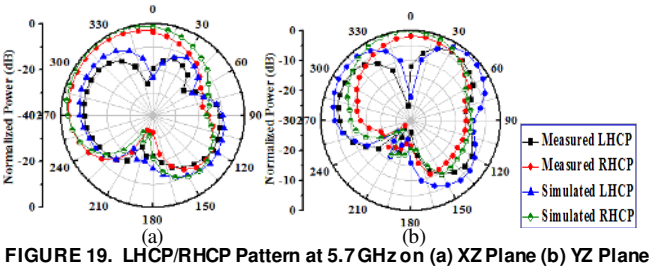

FIGURE 19. LHCP/RHCP Pattern at 5.7 GHz on (a) XZ Plane (b) YZ Plane

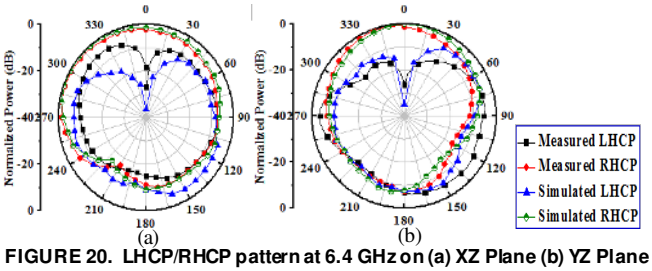

FIGURE 20. LHCP/RHCP pattern at 6.4 GHz on (a) XZ Plane (b) YZ Plane

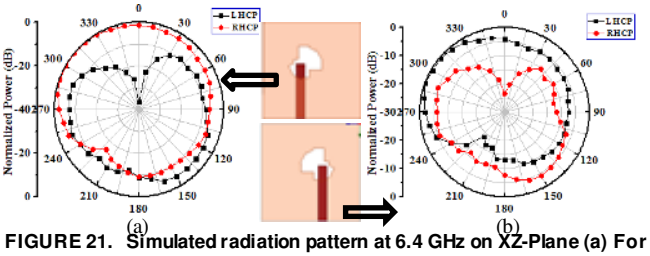

FIGURE 21. Simulated radiation pattern at 6.4 GHz on XZ-Plane (a) For RHCP operation (b) For LHCP operation

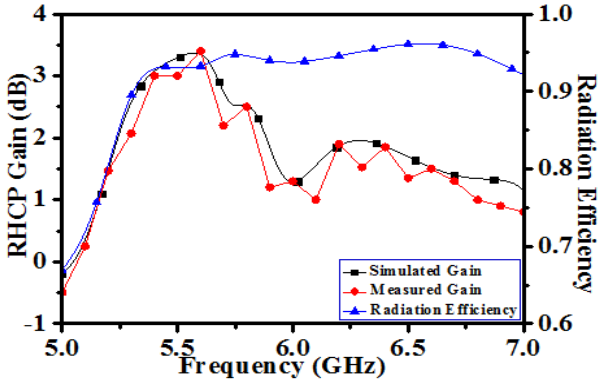

FIGURE 22. Simulated and measured RHCP gain and radiation efficiency response of the presented CP antenna at ($\theta = 0^0$ & $\phi = 0^0$)

This article has been accepted for publication in a future issue of this journal, but has not been fully edited. Content may change prior to final publication. Citation information: DOI 10.1109/ACCESS.2021.3093898, IEEE Access

TABLE VII CP PERFORMANCE OF THE PRESENTED ANTENNA IN COMPARISON WITH OTHER CP DRAs REPORTED EARLIER IN THE LITERATURE

DRA Shape	Feeding	ε_r	f_{cp} (GHz)	S_{11} (% & GHz)	BW_{CP} (% & GHz)	Gain (dBi)
Cylindrical DRA [21]	Annular slot with opposing stubs	9.5	1.96	18	3.4	4.5
Cylindrical DRA [22]	Circular shaped aperture	9.8	2.6/5.15	18.04 & (2.42-2.90)/ 19.85 & (4.9-5.68)	6.45 & (2.55-2.72)/ 14.74 & (4.9-5.68)	5.5/6
Four Rectangular Dielectric Layers [17]	Aperture coupling	10.2	9.5	21 & (8.9-11)	6 & (9.55-10.15)	6-6.7
Bow-tie shaped [6]	Asymmetric cross-slot	10.2	8.1	43.8 & (6.5-10.75)	7.4 & (7.8 – 8.4)	5.8
Cylindrical [This work]	Asymmetrical bow-tie shaped slot	9.8	5.5/6/6.5	26.73 & (5.25-6.87)	23.59 & (5.42-6.87)	3.4

V. CONCLUSIONS

In this paper, a circularly polarized slot-coupled cylindrical DRA excited by an off-centered microstrip line has been investigated for WLAN application. The proposed configuration achieved the measured impedance and CP bandwidth of 26.73% and 23.59%, respectively. The entire AR bandwidth has been covered the impedance frequency range and the complete AR frequency range is usable. The mirror image of the presented CP design switched the RHCP field into the LHCP field. The maximum RHCP gain of 3.4 dB has been delivered by the designed antenna.

REFERENCES

[1] A. Petosa, Dielectric Resonator Antenna Handbook. Norwood, MA, USA:Artech House, 2007.

[2] A. Perron, T. A. Denidni and A. R. Sebak, "Circularly polarized microstrip/elliptical dielectric ring resonator antenna for millimeter-wave applications", *IEEE Antennas and Wireless Propagation Letters*., vol. 9, pp. 783-786, 2010.

[3] Y. M. Pan, K. W. Leung and K. Lu, "Omnidirectional linearly and circularly polarized rectangular dielectric resonator antennas", *IEEE Transactions on Antennas and Propagation*, vol. 60, no. 2, pp. 751-759, 2012.

[4] K. W. Khoo, Y. X. Guo and L. C. Ong, "Wideband circularly polarized dielectric resonator antenna", *IEEE Transactions on Antennas and Propagation*, vol. 55, no. 7, pp. 1929-1932, 2007.

[5] G. Massie, M. Caillet, M. Clenet and Y. M. M. Antar, "A new wideband circularly polarized hybrid dielectric resonator antenna," *IEEE Antennas and Wireless Propagation Letters*, vol. 9, pp. 347-350, 2010.

[6] P. Chauthaiwale, R. K. Chaudhary and K. V. Srivastava, "Circularly polarized bowtie-shaped dielectric resonator antenna excited with asymmetric cross slot", *Microwave and Optical Technology Letters*, vol. 57, no. 7, pp. 1723 – 1727, 2015.

[7] W. C. Wong and K. W. Leung, "Circularly polarized dielectric resonator antenna excited by dual conformal strips of unequal lengths", *Microwave and Optical Technology Letters*, vol. 29, no. 5, pp. 348-350, 2001.

[8] Y. Pan, K. W. Leung and E. H. Lim, "Compact wideband circularly polarized rectangular dielectric resonator antenna with dual underlaid hybrid couplers", *Microwave Optical Technology Letters*, vol. 52, no. 12, pp. 2789–2791, 2010.

[9] E. H. Lim, K. W. Leung and X. S. Fang, "The compact circularly-polarized hollow rectangular dielectric resonator antenna with an underlaid quadrature coupler", *IEEE Transactions on Antennas and Propagation*, vol. 59, no. 1, pp. 288–293, 2011.

[10] K. K. Pang, H. Y. Lo, K. W. Leung, K. M. Luk and E. K. N. Yung, "Circularly polarized dielectric resonator antenna subarrays", Microwave and Optical Technology Letters, vol. 27, no. 6, pp. 377–379, 2000.

[11] S. L. S. Yang, R. Chair, A. A. Kishk, K. F. Lee and K. M. Luk, "Study on sequential feeding networks for subarrays of circularly polarized elliptical dielectric resonator antenna", IEEE Transactions on Antennas and Propagation, vol. 55, no. 2, pp. 321–333, 2007.

[12] M. Yang, Y. Pan and W. Yang, "A Singly Fed Wideband Circularly Polarized Dielectric Resonator Antenna," in IEEE Antennas Wireless Propagation Letters, vol. 17, no. 8, pp. 1515-1518,Aug.2018,doi:10.1109/LAWP.2018.2851574.

[13] S. Liu, D. Yang, Y. Chen, S. Huang and Y. Xiang, "Broadband Dual Circularly Polarized Dielectric Resonator Antenna for Ambient Electromagnetic Energy Harvesting," in IEEE Transactions on Antennas and Propagation, vol. 68, no. 6, pp. 4961-4966, June 2020,doi:10.1109/TAP.2020.2968768.

[14] W. Sun, W. Yang, P. Chu and J. Chen, "Design of a Wideband Circularly Polarized Stacked Dielectric Resonator Antenna," in IEEE Transactions on Antennas and Propagation, vol. 67, no. 1, pp. 591-595, Jan. 2019, doi: 10.1109/TAP.2018.2874678.

[15] M. Yang, Y. Pan, Y. Sun and K. Leung, "Wideband Circularly Polarized Substrate-Integrated Embedded Dielectric Resonator Antenna for Millimeter-Wave Applications," in IEEE Transactions on Antennas and Propagation, vol. 68, no. 2, pp. 1145-1150, Feb. 2020,doi:10.1109/TAP.2019.2938629.

[16] R. Chowdhary and R. K. Chaudhary, "An approach to generate circular polarization in a modified cylindrical shaped dielectric resonator antenna using PMC boundary approximation," *IEEE Antennas and Wireless Propagation Letters*, vol. 17, pp. 1727-1731, 2018.

[17] S. Fakhte, H. Oraizi and R. Karimian, "A novel low-cost circularly polarized rotated stacked dielectric resonator antenna," IEEE Antennas and Wireless Propagation Letters," *IEEE Antennas and Wireless Propagation Letters*, vol. 13, pp. 722-725, 2014.

[18] Y. Ding, K. W. Leung and K. M. Luk, "Compact circularly polarized dual band zonal-slot/DRA hybrid antenna without external ground plane", *IEEE Transactions on Antennas and Propagation*, vol. 59, no. 6, pp. 2404-2409, 2011.

[19] A. Sharma and R. K. Gangwar, "Compact dual-band ring shaped dielectric resonator antenna with moon shaped defected ground structure for WLAN/WiMAX applications," *International Journal of RF and Microwave Computer Aided Engineering*, vol. 26, pp. 503–511, 2016.

[20] P. Gupta, D. Guha and C. Kumar, "Dielectric resonator working as feed as well as antenna: new concept for dual-mode dual-band improved design" *IEEE Transactions on Antennas and Propagation*, vol. 64, pp. 1497-1502, 2016.

[21] K. W. Leung and S. K. Mok, "Circularly polarized dielectric resonator antenna excited by perturbed annular slot with backing cavity", Electronics Letters, vol. 37, pp. 934-936, 2001.

[22] A. Sharma, G. Das and R. K. Gangwar, "Dual-band circularly polarized modified circular aperture loaded cylindrical dielectric resonator antenna for wireless applications", Microwave and Optical Technology Letteres, vol. 59, pp. 1562–1570, 2017.

REENA KUMARI did her bachelor of engineering degree in Electronics and Communication Engineering from Birla Institute of Technology, Mesra, Ranchi, India in 2010 and Ph.D. degree in Electronics Engineering from the Indian Institute of Technology (Indian School of Mines), Dhanbad in the year 2019. Her research area is circularly polarized dielectric resonator antenna. She has authored over 11 research articles in international journal/conference proceedings. She has also served as a reviewer for IEEE Antennas and Wireless Propagation Letters and International Journal of RF Microwave and Computer Aided Engineering.

Ravi Kumar Gangwar received the B. Tech. degree in Electronics and Communication Engineering from U.P. Technical University, Lucknow and Ph.D. degree in Electronics Engineering from the Indian Institute of Technology, (Banaras Hindu University), Varanasi, India in 2006 and 2011 respectively.

He is currently Associate Professor in Department of Electronics Engineering and Associate Dean (Sponsored Research & Industrial Consultancy), at Indian Institute of Technology (Indian School of Mines) Dhanbad, India. He has authored or co-authored over 100 research papers in reputed international journals and 80 papers in conference proceedings. His research interest includes Dielectric Resonator Antenna, Microstrip Antenna and Bio-Electromagnetics. He is guided/guiding 15 Ph.D. and 19 M.Tech. students. He has completed/ongoing 08 R&D project (≈2 crores rupees) related Dielectric Resonator Antenna and their applications from various funding agencies like DRDO, SERB-DST, ISRO etc. He is recipient of INSA Visiting Scientist Fellowship and IETE Smt. Ranjana Paul Memorial Award for the year 2020.

He is a Senior Member of the Antenna and Propagation Society, Institute of Electrical and Electronics Engineers (IEEE), USA, Member, Institution of Engineering and Technology (IET) UK, Life Member of Institution of Engineers (IE) India and Fellow of Institution of Electronics and Telecommunication Engineers (IETE), India. He is also Member of IETE Executive Council and Joint Regional Secretary at Ranchi centre. He is also an external expert in peer review committee of project related to chaff application of Defence Laboratory Jodhpur, DRDO. He is also an Associate Editor of IEEE Access, IET Circuits Devices and Systems Journals. He is a reviewer of IEEE Transactions of Antenna and Propagation, IEEE Antenna and Propagation Letters, IEEE Antenna and Propagation Magazine, IET Microwave and Antenna Propagation, IET Electronics Letters, Microwave and Optical Technology Letters, Scientific Report etc.

.

RAGHVENDRA KUMAR CHAUDHARY Dr. Raghvendra Kumar Chaudhary is an Assistant Professor of the Department of Electronics Engineering, Indian Institute of Technology (ISM) Dhanbad, India. He received the B.Tech. from UIET Kanpur, India, in 2007, the M.Tech. from IIT(BHU) Varanasi, India, in 2009, and the PhD from IIT Kanpur, India in 2014. He has researched in developing the metamaterial antenna and dielectric resonator antenna (DRA). Development of the circularly polarized compact antenna is one of his major areas of contribution. He has published over 100 papers in top SCI Journals. Dr. Chaudhary has guided 04 PhD students and currently, 15 PhD students are working under him. He was a recipient of the Young Engineers Award (2020) of Indian National Academy of Engineering (INAE), Young Scientist Award (2020) of Institution of Electronics and Telecommunication Engineers (IETE), Young Engineers Award (2019-20) of Institution of Engineers, India (IEI) and many Best Paper awards in different categories in national & international conferences, such as IEEE APACE Malaysia, PIERS Singapore, and ATMS India. He has served as the Chair for the IEEE Student Branch of Uttar Pradesh Section, in 2012–2013 and currently serving as a counsellor of the IEEE Student Branch of IIT(ISM) Dhanbad. Dr. Chaudhary is serving as an Associate Editor of IET Microwave Antennas & Propagation, IEEE Access, and Microwave and Optical Technology Letters, Wiley. He is a Senior Member of IEEE and URSI, INAE Young Associate, and potential reviewer of international journals such as the IEEE Transactions on Antennas and propagation, the IEEE Antennas and Wireless Propagation Letters, etc. He has also been featured interviewed by IET Electronics Letters.